Observations of the (1→3)-β-D-Glucan Linear Triple Helix to Macrocycle Interconversion Using Noncontact Atomic Force Microscopy

Theresa M. McIntire and David A. Brant*

Contribution from the Department of Chemistry, University of California, Irvine, California 92697-2025

Received April 9, 1998

Abstract: The (1→3)-β-D-glucans (scleroglucan, schizophyllan, lentinan, etc.) are of interest for their immunostimulatory activity. The native polymer dissolves in water as very stiff and stable triple-stranded helices, which can be dissociated to single strand random coils by heating to 135 °C. When the single-stranded material is returned to temperatures favoring formation of the triple helix, various structures are formed depending on polymer concentration and thermal history. With suitable annealing at sufficiently low polymer concentration, much of the renatured material appears as macrocycles with diameters that can reach several tens of nanometers; under the same conditions, the remaining material adopts a stiff linear molecular architecture that strongly resembles the linear triple helical starting material. The relative numbers of linear and cyclic species and the respective distributions of contour lengths and thicknesses were measured as a function of the annealing temperature using noncontact atomic force microscopy. The ratio of cyclic to linear species declines from about 2 to 0.5 as the annealing temperature rises from 70 to 130 °C. The mean lengths and thicknesses of both species are essentially constant over the same temperature range, but both the mean contour length and mean thickness are greater for the linear than for the cyclic species. These results are interpreted qualitatively in terms of a model for the renatured material that recognizes in the multistranded cyclic species a free energetic advantage arising from a structural degeneracy lacking in the linear forms. This degeneracy compensates effectively for the energetic and entropic barriers to cycle formation in the multistranded aggregates.

Introduction

Source, Structure, and Applications of (1→3)-β-D-Glucans. Polymers of (1→3)-linked β-D-glucose are widely distributed in plants, fungi, bacteria, and yeast as structural components of cell walls or as reserve polysaccharides.[1] Scleroglucan is the name for capsular polysaccharides elaborated by various pathogenic plant fungi of the genus *Sclerotium*.[2] Schizophyllan, chemically identical to scleroglucan, is a cell wall component of the fungus *Schizophyllum commune*.[3]

The linear backbone of schizophyllan and scleroglucan is regularly substituted by β-(1→6)-D-glucose residues at OH(6) on every third main chain unit (Figure 1).[4] Molecular weights vary depending on the microorganism from which they are isolated and the method of preparation; reported weight-average molecular weights, M_w, range from 1×10^5 to 6×10^6 g/mol.[5,6] Solid-state (fiber) diffraction reveals a triple helix conformation with a pitch of 18 Å and six backbone glucose residues per helical turn in each single strand (Figure 2a); alignment of the strands in the helix is parallel.[4] The triple helix is stablized by interchain hydrogen bonds in which each backbone OH(2) serves as donor and acceptor to link it to OH(2) of a backbone glucose residue in each of the other two chains of the helix (Figure 2b). The (1→6)-linked β-D-glucopyranosyl side group substituents, not shown in Figure 2, protrude from the outside of the triple helix.[4]

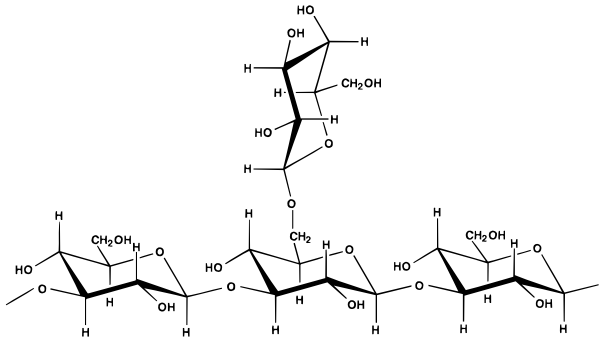

Figure 1. Repeating unit of scleroglucan and schizophyllan.

Scleroglucan and schizophyllan are popular model systems for rodlike or stiff wormlike chain behavior in aqueous solution,[7−9] because the triple helix is very stiff (persistence length ≈ 150 nm).[10] Their extended molecular conformation

(1) *Industrial Gums: Polysaccharides and Their Derivatives*, 3rd ed.; Whistler, R. L., BeMiller, J. N., Eds.; Academic Press: San Diego, CA, 1993; p 642.

(2) Johnson, J., Jr.; Kirkwood, S.; Misaki, A.; Nelson, T. E.; Scaletti, J. V.; Smith, F. *Chem. Ind. (London)* **1963**, 820−822.

(3) van der Valk, P.; Marchant, R.; Wessels, J. G. H. *Exp. Mycol.* **1977**, *1*, 69−82.

(4) Bluhm, T. L.; Deslandes, Y.; Marchessault, R. H.; Pérez, S.; Rinaudo, M. *Carbohydr. Res.* **1982**, *100*, 117−130.

(5) Rodgers, N. E. In *Industrial Gums: Polysaccharides and Their Derivatives*; 2nd ed.; Whistler, R. L., BeMiller, J. N., Eds.; Academic Press: San Diego, CA, 1973; pp 499−511.

(6) Sandford, P. A. In *Food Hydrocolloids*; Glicksman, M., Ed.; CRC Press: Boca Raton, FL, 1982; Vol. 1; pp 167−202.

(7) Sato, T.; Norisuye, T.; Fujita, H. *Carbohydr. Res.* **1981**, *95*, 195−204.

(8) Sato, T.; Norisuye, T.; Fujita, H. *Macromolecules* **1983**, *16*, 185−189.

S0002-7863(98)01203-7 CCC: $15.00
Published on Web 07/03/1998

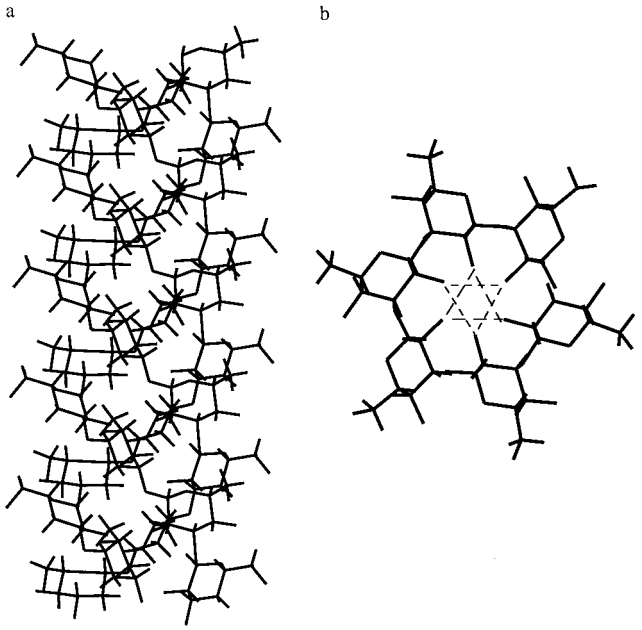

Figure 2. Computer-generated projections of the accepted triple helical structure of the (1→3)-β-D-glucans, specifically, hydrated crystalline Curdlan.[70] All hydroxyl hydrogens are deleted for clarity. (a) Side view showing triple helical entwinement of the chains normal to the molecular axis. (b) Cross sectional projection of two residues from each chain showing hydrogen bonding pattern experienced by OH(2) of every backbone glucose. The two triangular hydrogen-bonded networks are located at successive levels along the helix axis.

makes them interesting aqueous viscosity control agents, which are able to maintain their anisotropic form over wide ranges of tempertature, pH, and ionic strength.[5,6,11−15] The (1→3)-β-D-glucans are also immunoadjuvants of interest for their potential anticancer and/or antiviral properties.[16,17] Biological activity is related to the conformation of the (1→3)-β-D-glucan backbone, the molecular weight, and the presence of the (1→6)-β-D-glucosyl side chains.[1,17−22]

Conformational Transitions. Scleroglucan and schizophyllan are soluble in water and in dimethyl sulfoxide (DMSO). Measurements of mean molar mass, chain stiffness, and chain dimensions confirm that the polymer exists as a triple helix in water but as a single strand coil (unimer) in DMSO.[7,8,23−25] Conformational transitions of schizophyllan dissolved in water/DMSO mixed solvent solution have been mapped on a temperature−solvent composition "phase diagram" using scanning calorimetry to detect the conformational transitions (Figure 3).[26] In pure water, a reversible transition near 3 °C connects two triple helical morphologies, thought to differ in the organization of water localized in the vicinity of the triple helix.[27] This reversible low-temperature transition can be followed into the regime where the weight fraction of DMSO, w_D, approaches 0.87. In solvents still richer in DMSO, the triple helix is unstable relative to the single strand random coil. A high-temperature triple helix to random coil transition occurs near 130 °C in mixtures of water/DMSO with w_D less than about 0.70. This transition is not fully reversible by scanning calorimetry in this range of solvent composition. In solvent mixtures richer in DMSO, this phase boundary moves rapidly to lower temperatures with increasing DMSO and merges with the low-temperature phase boundary near $w_D = 0.87$, $T = 25$ °C.

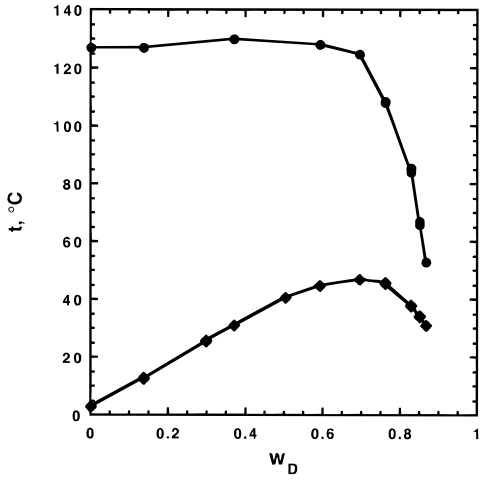

Figure 3. "Phase diagram" for schizophyllan in mixed DMSO−water solution. Calorimetrically measured temperatures of maximum excess heat capacity, t_p (◆), for sample U-1 are plotted vs the weight fraction of DMSO W_D.[26] The unmeasurable temperature of half-completion of the chain dissociation process $t_{1/2}$ (●) is estimated to be near 135 °C for $W_D > 0.5$. Constructed from data in the cited reference.

Denaturation, i.e., complete or partial triple strand separation, can be induced by crossing the upper phase boundary in Figure 3 with increasing T and/or w_D. Renaturation involves a crossing of this boundary from the random coil region into the domain of triple helix II. This can involve reduction in T at constant w_D or decrease in w_D (preferably by dialysis) at constant T or some combination of changes in T and w_D. To facilitate reorganization of the ordered helical structure in the renatured sample, it is desirable to anneal the sample under conditions close to the upper phase boundary.[28−31] Quenching from the annealing conditions to room temperature may be supposed to

(9) Yanaki, T.; Nishii, K.; Tabata, K.; Kojima, T. *J. Appl. Polym. Sci.* **1983**, *28*, 873−878.
(10) Stokke, B. T.; Brant, D. A. *Biopolymers* **1990**, 30, 1161−1181.
(11) Cottrell, I. W. In *Fungal Polysaccharides*; Sandford, P. A., Matsuda, K., Eds.; American Chemical Society: Washington, DC, 1980; pp 251−270.
(12) Holzwarth, G. *Dev. Ind. Microbiol.* **1985**, *26*, 271−280.
(13) Franz, G. *Planta Medica* **1989**, *55*, 493−497.
(14) Stokke, B. T.; Elgsæter, A.; Brant, D. A.; Kitamura, S. In *Physical Chemistry of Colloids and Interfaces in Oil Production*; Toulhoat, H., Lecourtier, J., Eds.; Editions Technip: Paris, 1992; pp 217−223.
(15) Brigand, G. In *Industrial Gums: Polysaccharides and Their Derivatives*; 3rd ed.; Whistler, R. L., BeMiller, J. N., Eds.; Academic Press: New York, 1993; pp 461−474.
(16) Jong, S.-C.; Donovick, R. *Adv. Appl. Microbiol.* **1989**, *34*, 183−262.
(17) Pretus, H. A.; Ensley, H. E.; McNamee, R. B.; Jones, E. L.; Browder, I. W.; Williams, D. L. *J. Pharm. Exp. Therap.* **1991**, *257*, 500−510.
(18) Singh, P. P.; Whistler, R. L.; Tokuzen, R.; Nakahara, W. *Carbohydr. Res.* **1974**, *37*, 245−247.
(19) Whistler, R. L.; Bushway, A. A.; Singh, P. P.; Nakahara, W.; Tokuzen, R. *Adv. Carbohydr. Chem. Biochem.* **1976**, *32*, 235−275.
(20) Yanaki, T.; Ito, W.; Tabata, K.; Kojima, T.; Norisuye, T.; Takano, N.; Fujita, H. *Biophys. Chem.* **1983**, *17*, 337−342.
(21) Kojima, T.; Tabata, K.; Itoh, W.; Yanaki, T. *Agric. Biol. Chem.* **1986**, *50*, 231−232.
(22) Bohn, J. A.; BeMiller, J. N. *Carbohydr. Polym.* **1995**, *28*, 3−14.
(23) Norisuye, T.; Yanaki, T.; Fujita, H. *J. Polym. Sci., Polym. Phys. Ed.* **1980**, *18*, 547−558.
(24) Yanaki, T.; Norisuye, T.; Fujita, H. *Macromolecules* **1980**, *13*, 1462−1466.
(25) Sato, T.; Sakurai, K.; Norisuye, T.; Fujita, H. *Polym. J.* **1983**, *15*, 86−96.
(26) Kitamura, S.; Kuge, T. *Biopolymers* **1989**, *28*, 639−654.
(27) Teramoto, A.; Gu, H.; Miyazaki, Y.; Sorai, M.; Mashimo, S. *Biopolymers* **1995**, *36*, 803−810.
(28) Stokke, B. T.; Elgsæter, A.; Brant, D. A.; Kitamura, S. *Macromolecules* **1991**, *24*, 6349−6351.
(29) Stokke, B. T.; Elgsæter, A.; Brant, D. A.; Kuge, T.; Kitamura, S. *Biopolymers* **1993**, *33*, 193−198.

trap the species distribution present under the annealing conditions;[32] annealing of native scleroglucan/schizophyllan at temperatures up to 100 °C yields no observable morphological changes in the linear triple helical material, suggesting that the kinetics of the reorganization process are slow for temperatures below 100 °C. We employ the term "native" to describe triple-stranded scleroglucan that has never been fully or partially dissociated (by heating or otherwise); "renatured" scleroglucan is material which has been denatured, annealed between the phase boundaries in Figure 3, and quenched to room temperature.

Morphology of the Renatured Material. The molecular architecture of scleroglucan/schizophyllan has been examined following denaturation/renaturation. Early dilute solution light scattering and hydrodynamic studies suggested that the triple helical structure could not be recovered following treatment at high T or high w_D.[8,23,33] More recently, the effects of heat treatment on more concentrated samples have been observed using ^{13}C NMR to discern clear differences in the gelling behaviors of heat-treated branched and unbranched (1→3)-β-D-glucans.[34] Muller and co-workers[35] used size exclusion chromatography to demonstate that thermal denaturation of the native triple helices of schizophyllan into random coils was complete after 10 min at 161 °C in neutral aqueous solution. They suggest also that no reassembly of the ordered forms occurs on return of the sample to room temperature.

Ultramicroscopy, in contrast to many physical methods that average over the sample population, is able to examine the morphology of individual molecules or molecular assemblies. Transmission electron microscopy (TEM) reveals linear, circular, and complex morphologies (multichain clusters or aggregates) in renatured scleroglucan/schizophyllan samples.[14,29−31,36] Aggregated structures predominate at higher polymer concentrations (> 1 mg/mL) and chain lengths. Novel circular polysaccharide structures with diameters of many nm are prominent in renatured samples of lower concentration. These circular structures do not form from native material that is too low in mean molar mass.[14,30] Atomic force microscopy (AFM) has recently proven an effective tool for examining biopolymer conformation.[32,37−53] We have shown, specifically, that non-contact atomic force microscopy (NCAFM) may be used to image renatured scleroglucan and other biological macromolecules.[32,54−56]

The present paper describes observations of the linear triple helix to macrocycle interconversion of scleroglucan, thermally denaturated in aqueous solution, renatured, and annealed near the high-temperature phase boundary. This transformation was studied as a function of annealing temperature, chain length, and polymer concentration using NCAFM to study the distribution and physical characteristics of the circular and linear species. The proportions of linear and cyclic species are investigated, the contour length distributions of the native and renatured macromolecular assemblies are measured, and the thickness of the assemblies is assessed by measuring the heights of the subject molecules on the mica surface.

Experimental Section

Preparation of Polysaccharide Solutions. Crude scleroglucan powder (Actigum CS 6, Lot No. 26, CECA S. A., Velizy, France) was suspended at 5 g/L in aqueous 0.02% sodium azide and stirred overnight at room temperature. The resulting turbid solution was centrifuged at 8000 rpm for 1.5 h to remove cell debris and unsolubilized polymer. Four aliquots (250 mL each) of the clear supernatant were sonicated (20 kHz, 375 W, 1/2 in. tip) at 0 °C for 1, 2, 3, and 4 h, respectively, centrifuged again as described, and filtered through 0.45 μm filters. The resulting clear solutions were then fractionally precipitated[57] with acetone to produce fractions of differing mean molar mass. Each fraction was redissolved separately in water, dialyzed exhaustively against distilled water, and recovered by freeze-drying. Precipitated fractions were designated *h*P*n*, where $h = 1$, 2, 3, or 4 designates the hours of sonication and $n = 1$, 2, 3, ... designates the fraction number from the acetone precipitation. Increasing values of n imply sequentially later fractions collected at higher acetone concentrations. Unsonicated, unfractionated scleroglucan (designated fraction 0P1) was also investigated. Fractions chosen for study were redissolved in distilled water at 1 mg/mL. Previously purified schizophyllan (designated fraction 0P2) was kindly provided by Dr. Kengo Tabata (Taito Co., Ltd., Tokyo, Japan). It was dissolved in water at approximately 1 mg/mL and used without further processing.

Some of the redissolved scleroglucan fractions were exposed to a denaturation−renaturation procedure: Aliquots in sealed 10 mL microreaction vials were first heated to 160 °C for 15 min in a thermostated oil bath to dissociate the native triple helix.[26,35] The vials were then placed in a thermostated oil bath at some predetermined temperature below 160 °C, annealed at constant temperature for various times, and quenched to room temperature in an ice bath. Most of the annealing temperatures were below the nominal transition temperature ($T_m \approx 135$ °C). Some of the annealing temperatures were above T_m,

(30) Stokke, B. T.; Elgsæter, A.; Kitamura, S. *Int. J. Biol. Macromol.* **1993**, *15*, 63−68.
(31) Kitamura, S.; Hirano, T.; Takeo, K.; Fukada, H.; Takahashi, K.; Falch, B. H.; Stokke, B. T. *Biopolymers* **1996**, *39*, 407−416.
(32) McIntire, T. M.; Penner, R. M.; Brant, D. A. *Macromolecules* **1995**, *28*, 6375−6377.
(33) Norisuye, T. *Makromol. Chem. Suppl.* **1985**, *14*, 105−118.
(34) Adachi, Y.; Ohno, N.; Yadomae, T.; Suzuki, Y.; Ohsawa, M.; Oikawa, S. *Carbohydr. Res.* **1990**, *198*, 111−122.
(35) Zentz, F.; Verchère, J.-F.; Muller, G. *Carbohydr. Polym.* **1992**, *17*, 289−297.
(36) Stokke, B. T.; Elgsæter, A. In *Advances in Carbohydrate Analysis*; White, C. A., Ed.; JAI Press, Ltd.: London, 1991; Vol. 1; pp 195−247.
(37) Drake, B.; Prater, C. B.; Weisenhorn, A. L.; Gould, S. A. C.; Albrecht, T. R.; Quate, C. F.; Cannell, D. S.; Hansma, H. G.; Hansma, P. K. *Science* **1989**, *243*, 1586−1589.
(38) Engel, A. *Annu. Rev. Biophys. Biophys. Chem.* **1991**, *20*, 79−108.
(39) Bustamante, C.; Vesenka, J.; Tang, C. L.; Rees, W.; Guthold, M.; Keller, R. *Biochemistry* **1992**, *31*, 22−26.
(40) Hansma, H. G.; Vesenka, J.; Siegerist, C.; Kelderman, G.; Morrett, H.; Sinsheimer, R. L.; Elings, V.; Bustamante, C.; Hansma, P. K. *Science* **1992**, *256*, 1180−1184.
(41) Bustamante, C.; Keller, D.; Yang, G. *Current Opin. Struct. Biol.* **1993**, *3*, 363−372.
(42) Lindsay, S. M. In *Scanning Tunneling Microscopy: Theory, Techniques and Applications*; Bonnell, D. A., Ed.; VCH Press: New York, 1993.
(43) Morris, V. J. *Prog. Biophys. Mol. Biol.* **1994**, *61*, 131−185.
(44) Braunstein, D. *J. Vac. Sci. Technol. A* **1995**, *13*, 1733−1736.
(45) Kirby, A. R.; Gunning, A. P.; Morris, V. J. *Carbohydr. Res.* **1995**, *267*, 161−166.
(46) Kirby, A. R.; Gunning, A. P.; Morris, V. J.; Ridout, M. J. *Biophys. J.* **1995**, *68*, 360−363.
(47) Morris, V. J.; Kirby, A. R.; Gunning, A. P. *Food Hydrocolloids* **1995**, *9*, 273−280.
(48) Kirby, A. R.; Gunning, A. P.; Morris, V. J. *Biopolymers* **1996**, *38*, 355−366.
(49) Gunning, A. P.; Kirby, A. R.; Morris, V. J. *Ultramicroscopy* **1996**, *63*, 1−3.
(50) Gunning, A. P.; Kirby, A. R.; Ridout, M. J.; Brownsey, G. J.; Morris, V. J. *Macromolecules* **1996**, *29*, 6791−6796.
(51) Gunning, A. P.; Morris, V. J.; Al-Assaf, S.; Phillips, G. O. *Carbohydr. Polym.* **1996**, *30*, 1−8.
(52) Round, A. N.; MacDougall, A. J.; Ring, S. G.; Morris, V. J. *Carbohydr. Res.* **1997**, *303*, 251−253.
(53) Morris, V. J.; Gunning, A. P.; Kirby, A. R.; Round, A.; Waldron, K.; Ng, A. *Int. J. Biol. Macromol.* **1997**, *21*, 61−66.
(54) Brant, D. A.; McIntire, T. M. In *Large Ring Molecules*; Semlyen, J. A., Ed.; Wiley: Chichester, England, 1996; pp 113−154.
(55) McIntire, T. M.; Brant, D. A. In *Techniques in Glycobiology*; Townsend, R. R., Hotchkiss, A. T., Eds.; Marcel Dekker: New York, 1997; pp 187−208.
(56) McIntire, T. M.; Brant, D. A. *Biopolymers* **1997**, *42*, 133−146.
(57) Kotera, A. In *Polymer Fractionation*; Cantow, M. J. R., Ed.; Academic Press: New York, 1967; pp 43−66.

Table 1. Characteristics of Experimental Samples[a]

sample	L_n, nm	M_w, g/mol	M_w/M_n	method[b]
0P1	578.4 ± 567.9 (333)	2.43×10^6	1.96	NCAFM
0P1		1.84×10^6		LS
1P2	385.0 ± 243.9 (319)	1.13×10^6	1.40	NCAFM
2P2	315.3 ± 174.2 (225)	8.80×10^5	1.30	NCAFM
3P3	184.9 ± 97 (287)	5.03×10^5	1.27	NCAFM
3P3		3.77×10^5	1.18	GPC w/RALLS & [η] detectors
3P3		4.87×10^5	1.48	GPC w/MALLS
4P2	215.9 ± 121.2 (370)	6.07×10^5	1.31	NCAFM
4P2		6.33×10^5		LS

[a] Weight average molecular weights and polydispersities (M_w and M_w/M_n) and the number average contour lengths (L_n) of these samples are listed along with the methods used to determine these characteristics. Standard deviations of L_n are quoted as are the numbers of molecules contributing to the average in the NCAFM measurements (in parentheses). [b] LS = lightscattering; RALLS = right-angle laser LS; MALLS = multi-angle laser LS; GPC = gel permeation chromatography.

in which cases the annealing process cannot be said to have been carried out under renaturing conditions. Nevertheless, we refer to the generic sequence of heating to 160 °C, annealing, and quenching to room temperture as a denaturation−renaturation process.

The dependence of the experimental observables on annealing temperature was examined for samples 0P1, 1P2, 2P2, 3P3, and 4P2, all of which had different mean degrees of polymerization as determined by NCAFM and/or conventional solution measurements. The dependence of the observables on annealing time was investigated with fraction 3P3. The weight average molecular weights and polydispersities (M_w and M_w/M_n) and the number average contour lengths (L_n) of these samples are listed in Table 1 along with the methods used to determine these characteristics. Standard deviations of L_n are quoted as are the numbers of molecules contributing to the average (in parentheses).

Preparation of Samples for Microscopy. Polysaccharide stock solutions, prepared as described above at approximately 1 mg/mL, were diluted with distilled water to a final polymer concentration of 4−30 μg/mL. Aliquots of these diluted solutions were deposited by spraying a fine aerosol[32,56,58−60] onto freshly cleaved mica (Polysciences, Inc., Warrington, PA) and air-dried. Mica is easily prepared by cleaving with tape and provides an atomically flat substrate free of artifacts found on other commonly used scanning probe microscopy substrates such as highly oriented pyrolytic graphite. After air-drying for a few hours, samples were imaged by NCAFM.

Imaging Procedures. Specimens were examined using a Park Scientific AutoProbe CP scanning probe microscope equipped with an NCAFM probe head. A piezoelectric scanner with a range up to 10 μm was used for all images. The scanner was calibrated in the *xy* directions using a 1.0 μm grating and in the *z* direction using several conventional height standards.[32,55,56] The tips used were V-shaped silicon 2 μm cantilevers (Ultralevers, Model No. APUL-20-AU-25, Park Scientific Instruments) with a force constant of 13 N/m and resonant frequency ω_0 of approximately 280 kHz. The oscillation frequency ω of the cantilever/tip was offset from ω_0 to higher frequencies by a few kHz to achieve maximal sensitivity.[32,44,55] The oscillation amplitude and *z* direction set point were adjusted to avoid tip−sample contact according to the operating procedures for noncontact mode imaging. Tip fouling events were infrequent, and any given sample could be imaged repeatedly with no evidence of sample disruption by contact with the tip. All measurements were performed in air at ambient pressure and humidity. Images were stored as 256 × 256 point arrays and analyzed using AutoProbe image processing software supplied by Park Scientific Instruments.

Imaging Observables. The numbers of linear and cyclic clusters present in each micrographic field were counted, and the contour lengths and thicknesses of individual clusters were measured. For linear species without significant bends, the contour length was calculated from the coordinates of the termini of the cluster. Bent linear clusters were subdivided approximately into straight segments, and the contour length of the cluster was taken as the sum of the lengths of the component segments. We estimate that the coordinates of the ends of linear clusters or segments of linear clusters can be specified to within ±5 nm to produce a random error of ±10 nm in the measured contour lengths of individual linear clusters. The contour length of cyclic clusters was taken as π times the length of the diameter of the cluster, measured along the scan direction. These diameters were measured between points of maximum height on the two limbs of the cluster connected by the diameter. We estimate that these points can be specified to within ±2.5 nm so that the contour lengths of individual cyclic clusters carry a random error of ±15 nm. Possible systematic errors are discussed in the final section of the paper.

The thickness of a cluster, measured in the direction normal to the mica substrate, was determined from the profile of a single scan across the cluster near the center of the cluster. Cluster thicknesses measured from many different scan profiles for the same cluster yield ratios of the standard deviation to the mean thickness in the range of 0.05−0.30. We have chosen at this stage to gather thickness data from single arbitrary scans through as many clusters as possible rather than assemble data from multiple measurements on a given cluster. Anywhere from 5 to 50 separate micrographic fields, containing a total of 100−400 clusters, were examined for each scleroglucan sample investigated. Contour length and thickness distribution functions were assembled for each class of cluster (linear and cyclic) for each scleroglucan sample studied.

The following symbols are used to denote mean values of the observables calculated from the distributions for each scleroglucan sample and, for the renatured samples, for each annealing temperature:

^{l}L = mean contour length of linear structures averaged over linear clusters of a given sample

^{c}L = mean contour length of cyclic structures averaged over cyclic clusters of a given sample

^{l}T = mean thickness of linear structures averaged over linear clusters of a given sample

^{c}T = mean thickness of cyclic structures averaged over cyclic clusters of a given sample

N^{l} = number fraction of linear structures computed over all clusters of a given sample

N^{c} = number fraction of cyclic structures computed over all clusters of a given sample

$L_n = N^{ll}L + N^{cc}L$ = number average contour length of linear and cyclic structures of a given sample

$T_n = N^{ll}T + N^{cc}T$ = number average thickness of linear and cyclic structures of a given sample

This notation is adapted from that used in a theoretical description of the current system.[54,61] The quantities ^{l}L, ^{c}L, ^{l}T, and ^{c}T are all simple arithmetic means averaged over the populations of linear and cyclic structures, respectively, as signified by upper left superscripts. Structures that cannot be classified as linear or cyclic are ignored in accumulating the data represented by the above notation. In most cases of interest here, such structures represent a small proportion, usually <10%, of the material observable in the NCAFM topographs. Number fractions N^{l} and N^{c} are reckoned relative to the entire population of clusters, hence, the upper right superscripts.

Results and Discussion

Illustration of NCAFM Observables. Figure 4 shows an NCAFM image of unsonicated native scleroglucan fraction 0P1 applied by aerosol spray deposition to mica as a 7.0 μg/mL solution in pure water. The excellent spatial separation of the molecules in this figure is typical of images prepared as described above and readily permits measurement of the observables just mentioned.[55,56] The number average contour length $L_n = {}^{l}L = 578.4 \pm 567.9$ nm for a sample of 333

(58) Tyler, J. M.; Branton, D. *J. Ultrastruct. Res.* **1980**, *71*, 95−102.
(59) Stokke, B. T.; Elgsæter, A.; Smidsrød, O. *Int. J. Biol. Macromol.* **1986**, *8*, 217−225.
(60) Stokke, B. T.; Elgsæter, A. *Micron* **1994**, *25*, 469−491.
(61) Gascoigne, L. W. Baccalaureate Honors Thesis, University of California, Irvine, 1996.

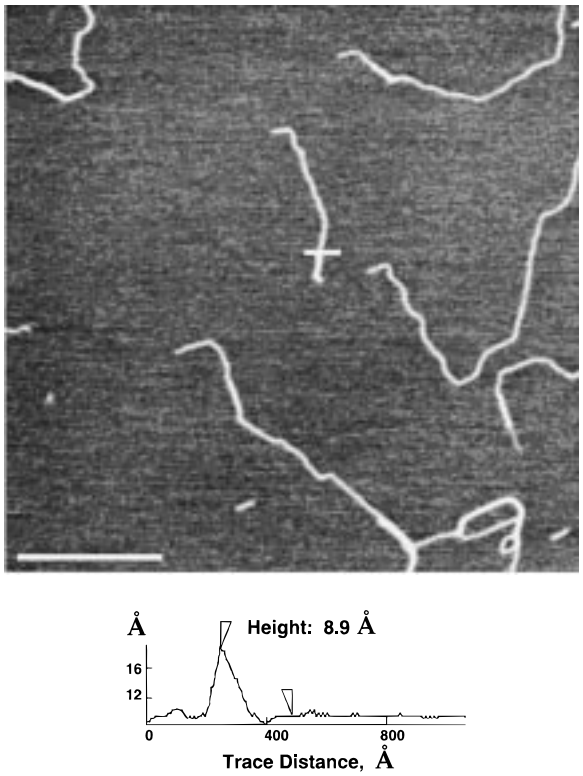

Figure 4. (top) NCAFM image of unsonicated native scleroglucan fraction 0P1 applied by aerosol spray deposition to mica as a 7.0 μg/mL solution in pure water. Scale bar = 400 nm. (bottom) Trace across one scleroglucan chain shown above as horizontal white bar.

molecules contained in about 45 separate images. All numbers following the ± sign in what follows represent one standard deviation for the distribution of molecules sampled, unless otherwise specified. Assuming that the accepted mass per unit length of triple helical scleroglucan (M_L = 2140 daltons/nm)[4,62] applies to these structures, this length distribution corresponds to number and weight average molar masses $M_n = 1.24 \times 10^6$ and $M_w = 2.43 \times 10^6$, respectively. We assume this M_L throughout to interconvert NCAFM observations to M_n and M_w; in cases where comparisons with solution measurements of molar mass are available (native samples only), the agreement is excellent (Table 1).[56] Images obtained with native schizophyllan fraction 0P2, which has the same repeating unit, are very similar to Figure 4.[56]

Tracings across individual scleroglucan molecules illustrate the ability of NCAFM to measure the thickness of macromolecular chains normal to the surface of the mica substrate. An example is shown in Figure 4. The measured mean thicknesses of unsonicated native scleroglucan 0P1 and schizophyllan 0P2 are $T_n = {}^1T = 1.14 \pm 0.30$ nm and 1.08 ± 0.27 nm, respectively, averaged over hundreds of molecules. X-ray diffraction analysis of partially crystalline scleroglucan fibers drawn from concentrated aqueous solution yields a model for crystalline scleroglucan with a center-to-center spacing of 1.73 nm between scleroglucan triple helices aligned in parallel hexagonal array.[4] Our results for T_n of 0P1 and 0P2 are therefore approximately 65% of the triple strand thickness expected from X-ray diffraction.[4] This discrepancy in expected chain thickness is typical of many other systems which have been investigated;[32,56,63] its origins are under investigation. We demonstrate in what follows that this apparent error in measured chain thickness does not preclude meaningful observation of systematic differences in chain thickness between linear and circular scleroglucan structures that occur in the renatured samples. AFM methods do not yield reliable chain thicknesses measured parallel to the substrate surface, because the molecular chain thickness is convoluted with the thickness of the AFM probe.[41]

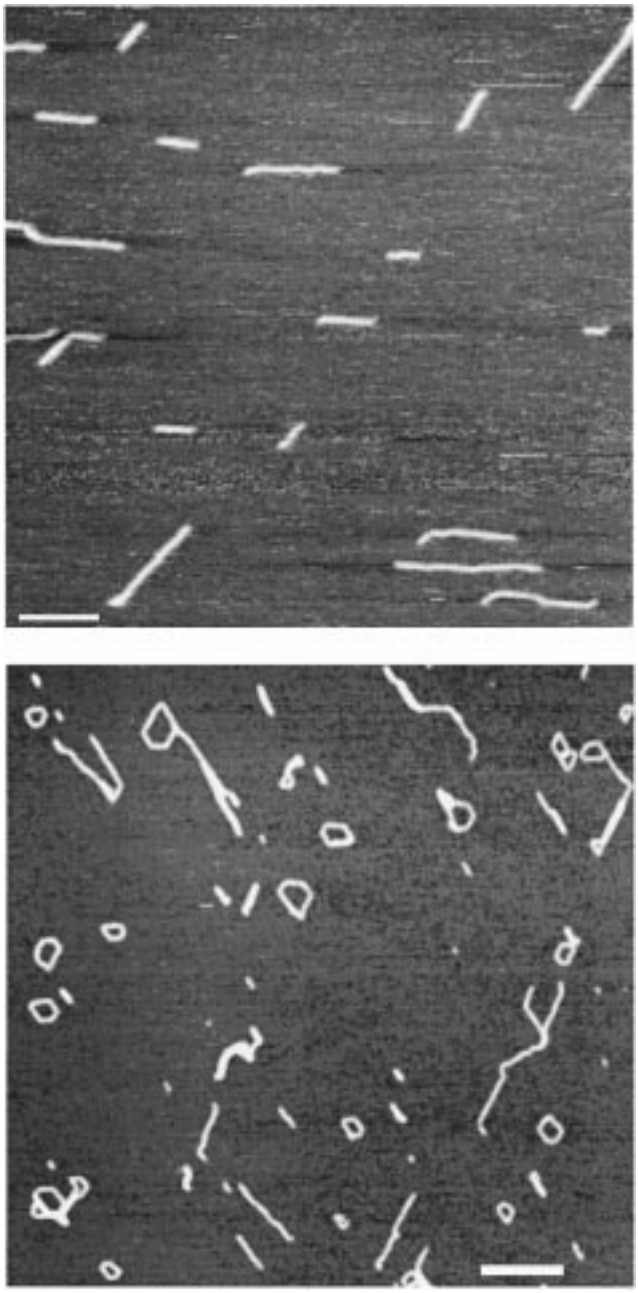

Figure 5. (top) NCAFM image of a native sample of fraction 4P2 scleroglucan. Scale bar = 200 nm. (bottom) A representative NCAFM image of scleroglucan fraction 4P2 after it has been subjected to denaturation at 160 °C for 15 min, annealed at 90 °C for 4 h, and quenched to room temperature. Scale bar = 200 nm.

Lower molecular weight fractions of scleroglucan were obtained by ultrasonication and fractional precipitation as described above, so that the dependence of scleroglucan cyclization on chain length could be investigated. Fractions 1P2, 2P2, 3P3, and 4P2 were selected for study. A native sample of fraction 4P2 is imaged in Figure 5 (top), where its smaller chain length relative to fraction 0P1 is evident. Preferential alignment of the chains is quite obvious in this figure. This tendency, evident in many of the micrographs, may

(62) Yanaki, T.; Norisuye, T. *Polym. J.* **1983**, *15*, 389−396.
(63) Müller, D. J.; Engel, A. *Biophys. J.* **1997**, *73*, 1633−1644.

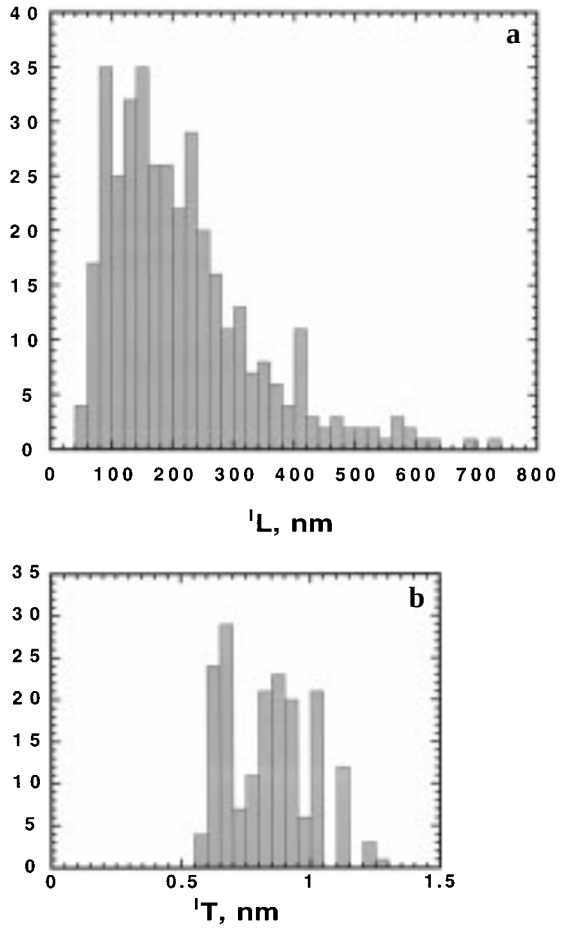

Figure 6. (a) Contour length distribution for scleroglucan fraction 4P2 molecules some of which are shown in Figure 5 (top). (b) Thickness distribution for scleroglucan 4P2 molecules some of which are shown in Figure 5 (bottom).

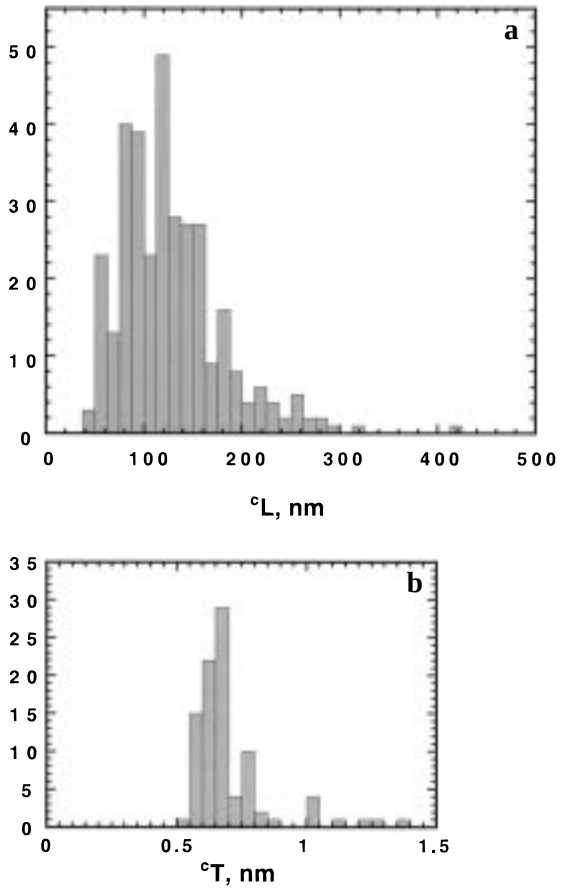

Figure 7. (a) Circle contour length distribution for scleroglucan fraction 4P2, denatured at 160 °C for 15 min, annealed at 90 °C for 4 h, and quenched to room temperature. (b) Circle thickness distribution for scleroglucan fraction 4P2, denatured at 160 °C for 15 min, annealed at 90 °C for 4 h, and quenched to room temperature.

be due to drying artifacts[64] or to effects arising from interactions of the molecules with features of the underlying mica substrate.[32] For native fraction 4P2 the number average contour length $L_n = {}^lL = 215.9 \pm 121.2$ nm, averaged over 370 molecules in about 40 micrographs. The distributions of chain lengths and thicknesses for this sonicated native fraction are shown as histograms, in Figure 6a and 6b, respectively.

The mean contour length $L_n = {}^lL$ of native 4P2 corresponds to $M_n = (4.62 \pm 2.59) \times 10^5$ daltons, and the distribution of lengths yields $M_w/M_n = 1.31$ for the polydispersity index. This result agrees well with $M_w = (6.33 \pm 0.28) \times 10^5$ obtained from light scattering experiments (Table 1). The observed polydispersity index indicates that scleroglucan fraction 4P2 contains a relatively narrow distribution of chain lengths. The sonication and fractionation procedures described above consistently produce values of M_w/M_n in the range of 1.3 without excessive effort. The mean scleroglucan chain thickness $T_n = {}^lT$ for this sonicated, but native, linear sample is 0.83 ± 0.16 nm, which is significantly smaller than the mean thicknesses measured for fractions 0P1 and 0P2. The general observation that the sonicated native samples are thinner than the unsonicated native material is addressed further below.

Figure 5 (bottom) shows a representative image of fraction 4P2 after it has been subjected to denaturation at 160 °C for 15 min, annealed at 90 °C for 4 h, and quenched to room temperature. The micrograph displays linear species and several circles, some of which may be supercoiled (the "figure eight" structures).[28] For some 151 linear and 335 cyclic molecules observed following renaturation of sample 4P2, the mean contour lengths are, respectively, ${}^lL = 130 \pm 95$ nm and ${}^cL = 127 \pm 52$ nm. It is very typical of sonicated renatured samples that ${}^cL < {}^lL$; usually the difference is considerably larger than reported here for fraction 4P2, and such differences are statistically significant (see below). The average thicknesses of the denatured and annealed linear and cyclic helices are ${}^lT = 0.83 \pm 0.23$ nm and ${}^cT = 0.70 \pm 0.16$ nm, respectively. We find consistently that ${}^cT < {}^lT$ by statistically significant amounts in samples that have been renatured. On the other hand, ${}^lT$ for the renatured sonicated samples is usually at least 95% of ${}^lT = T_n$ for the corresponding linear native material. Figure 7 illustrates the distributions of contour lengths and chain thickness that characterize the cyclic species in a renatured sample, here 4P2.

The number average molar mass of all material recovered following denaturation and annealing of 4P2 is $M_n = (2.74 \pm 1.40) \times 10^5$ Da. This is to be compared with $(4.62 \pm 2.59) \times 10^5$ for the native 4P2. Because we see no evidence of chain degradation at elevated annealing temperatures over many hours (see below), we believe that the apparent reduction in molar mass relative to the undenatured material is probably due to the existence of some "nicks" in the strands comprising the undenatured triple helices. Our observations of thermal stability of the scleroglucan strands seemingly contradict earlier reports,[34,35] and it remains possible that some thermal degradation occurs during the 15 min period that our samples are subjected

(64) Wilkins, M. J.; Davies, M. C.; Jackson, D. E.; Roberts, C. J.; Tendler, S. J. B. *J. Microscopy* **1993**, *172*, 215−221.

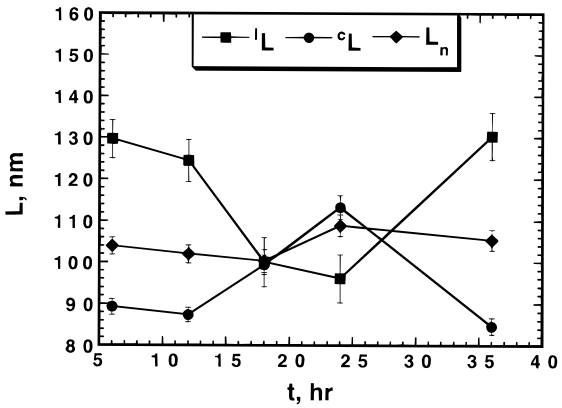

Figure 8. A plot of the contour lengths ^{l}L (■), ^{c}L (●), and L_n (◆) versus annealing time at 70 °C for 3P3 after denaturation at 160 °C for 15 min in water (error bars are standard errors, defined as standard deviation/sample size).

to thermal dissociation at 160 °C. The ratio of about 2 observed for L_n for the native sonicated samples relative to the renatured sonicated samples suggests the presence of about one nick per single strand chain in the native sonicated samples. This conclusion assumes, of course, that the detailed structure and M_L of the native and renatured species are essentially identical. This assumption might well be questioned, given the reported differences in contour length and strand thickness for renatured cyclic and linear structures.

Dependence of NCAFM Observables on Annealing Time. Dependence of the observables on annealing time was examined using fraction 3P3 at annealing temperatures of 70 and 120 °C. Figure 8 shows plots of the contour lengths ^{c}L, ^{l}L, and L_n versus annealing time at 70 °C for 3P3 after denaturation at 160 °C for 15 min in water. Alhough ^{l}L and ^{c}L display rather large variations with time after about 12 h, the number weighted average over all species, L_n, shows no evidence of any chain degradation with time at 70 °C. Data collected at 120 °C showed similiar results. Measurements were made by sampling from a single annealing experiment as a function of time. Note that sample sizes for the cyclic and linear species are only about half that for the combined result, so the statistics for ^{l}L and ^{c}L are poorer than those for L_n.

After very long annealing times (≥18 h), the micrographs revealed many multichain clusters and large aggregates of linear and cyclic material (data not shown). In some such samples precipitated material was visible to the eye. Chain aggregation may have occurred at long annealing times due to hydrolysis of the (1→6)-*β*-D-glucose side chains. This would convert the polymer to the unbranched (1→3)-D-glucan, Curdlan, which is known to gel.[65] In view of the evidence that no sensible changes occur in ^{l}L, ^{c}L, and L_n until much longer times, we have chosen an annealing time of 4 h for most investigations of the dependence of the observables on annealing temperature and chain length reported here.

Dependence of NCAFM Observables on Annealing Temperature and Chain Length. We have examined the dependence of the NCAFM observables on the annealing temperature using scleroglucan samples 0P1, 1P2, 2P2, 3P3, and 4P2. Unless otherwise noted, the denatured samples were prepared by heating to 160 °C for 15 min, annealing for 4 h at the indicated temperature, and quenching to room temperature for observation. Figure 9 shows the ratio N^c/N^l plotted against annealing temperature for all of the above samples. The

(65) Maeda, I.; Saito, H.; Masada, M.; Misaki, A.; Harada, T. *Agric. Biol. Chem.* **1967**, *31*, 1184−1188.

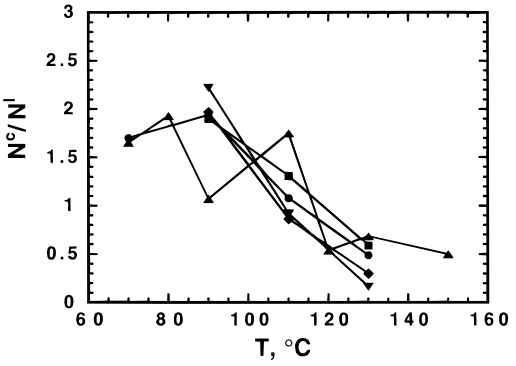

Figure 9. Plot of the ratio N^c/N^l plotted against annealing temperature for all scleroglucan samples [0P1 (●), 1P2 (■), 2P2 (◆), 3P3 (▲), and 4P2 (▼)].

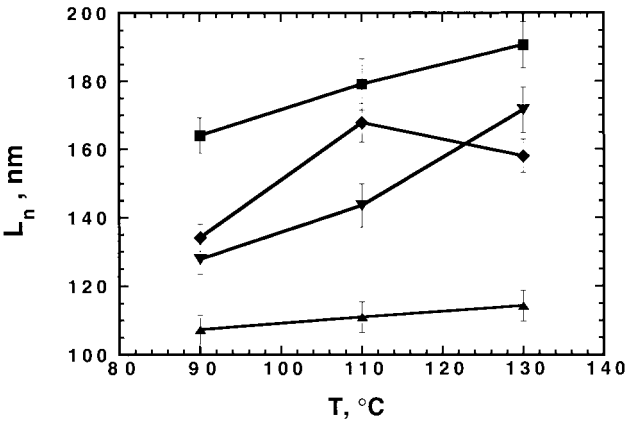

Figure 10. Plot of L_n against annealing temperature for renatured samples 1P2 (■), 2P2 (◆), 3P3 (▲), and 4P2 (▼) (error bars are standard errors).

temperature dependence of this ratio shows remarkably similar behavior for all of the samples, whose weight average molar masses range from about 4×10^5 to about 2.4×10^6. The number ratio of cyclic to linear structures varies from about 2 at 90 °C to about 0.5 at 130 °C. Data for samples 3P3 and 0P1 extend beyond this temperature range and generally reinforce the conclusions based on the range 90 °C ≤ T ≤ 130 °C.

The observed noise in the plot of the N^c/N^l population ratio vs T is not unexpected in view of the sampling statistics; each point results from counting cyclic and linear structures in samples of several hundred observed structures. In addition to random noise from the small sample size, there may be some more systematic sampling error arising from the need to classify the observed structures as cyclic or linear. Structures for which a classification could not be made unabiguously were simply not included in the tabulations. Despite the somewhat noisy measure of the population ratio, the similarity of behaviors among the several samples studied suggests that the absolute value of the ratio and its decline with increasing T are both reliable.

The dependence of L_n on annealing temperature is shown in Figure 10 for renatured samples 1P2, 2P2, 3P3, and 4P2. These sonicated and fractionated samples display distinctly different number average contour lengths, all of which increase with increasing annealing temperature. While the trend of the temperature dependence might not be convincing for any one of these samples, the uniformity of their behavior makes the increase of L_n with annealing temperature quite unmistakable. When ^{l}L and ^{c}L are examined separately, a statistically significant difference in the contour lengths of the linear and

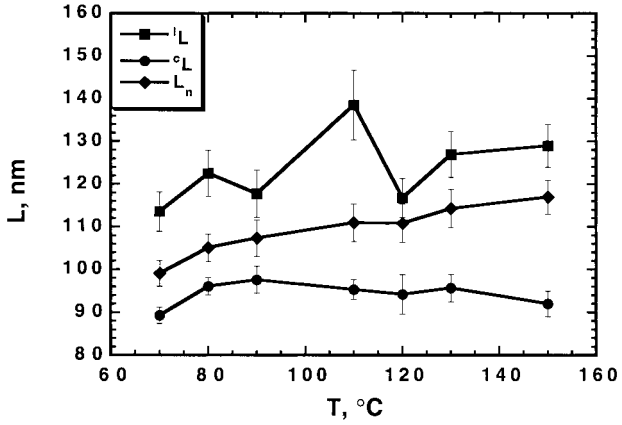

Figure 11. Plot of ^{l}L (■), ^{c}L (●), and L_n (◆) versus annealing temperature for all experiments for scleroglucan sample 3P3 (error bars are standard errors).

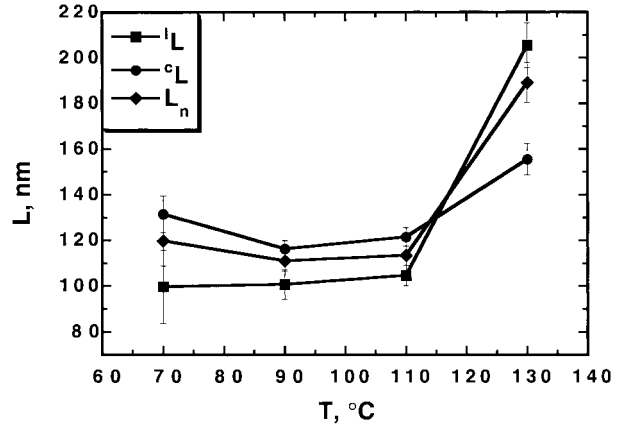

Figure 12. Plot of ^{l}L (■), ^{c}L (●), and L_n (◆) against annealing temperature for the renatured unsonicated and unfractionated sample 0P1 (error bars are standard errors).

cyclic species is observed; the linear species invariably have mean contour lengths greater than the cyclic species. This observation is shown in Figure 11, where data for renatured samples 3P3 are presented. These results are representative of what is observed with the other sonicated and fractionated samples.

Figure 12 presents ^{l}L, ^{c}L, and L_n against annealing temperature for the renatured unsonicated and unfractionated sample 0P1. The upward trend of contour length with annealing temperature is seen again, but in this case $^{c}L > {}^{l}L$ over most of the temperature range investigated. Notice that the ratio of L_n for the native material to that for the renatured material is almost 5, which suggests that the native unsonicated material contains more single-stranded nicks than the sonicated native material for which this ratio is closer to 2. Unsonicated samples were denatured at 160 °C for 30 rather than 15 min and at 0.5 mg/mL instead of 1 mg/mL because of a tendency of this higher molecular weight material to denature more slowly and to form larger aggregates upon renaturation.

Figure 13 shows ^{l}T and ^{c}T as functions of annealing temperature for renatured samples 1P2, 2P2, 3P3, and 4P2. In contrast to the contour lengths, the observed thickness for these sonicated, renatured samples do not show any detectable dependence on sonication time (mean molar mass) or annealing temperature. The mean thicknesses $\langle {}^{l}T \rangle$ and $\langle {}^{c}T \rangle$ averaged over all molecular weights and annealing temperatures are 0.83 ± 0.20 nm and 0.68 ± 0.14, respectively. This difference is statistically significant at the 97% confidence level. Plots of

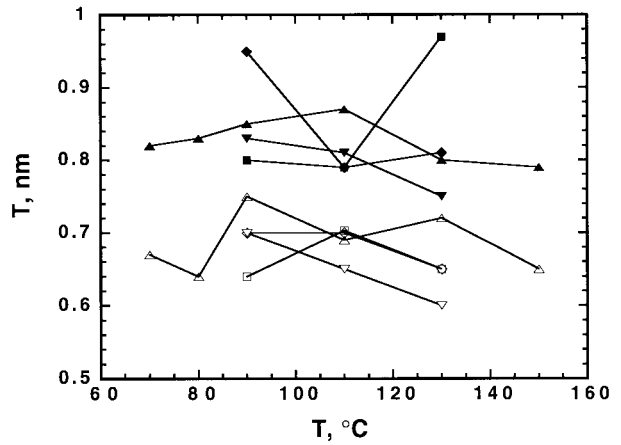

Figure 13. Plot of species thickness, T, [^{l}T and ^{c}T] as a function of annealing temperature for renatured samples 1P2 [^{l}T (■), ^{c}T (□)], 2P2 [^{l}T (◆), ^{c}T (◇)], 3P3 [^{l}T (▲), ^{c}T (△)], and 4P2 [^{l}T (▼), ^{c}T (▽)].

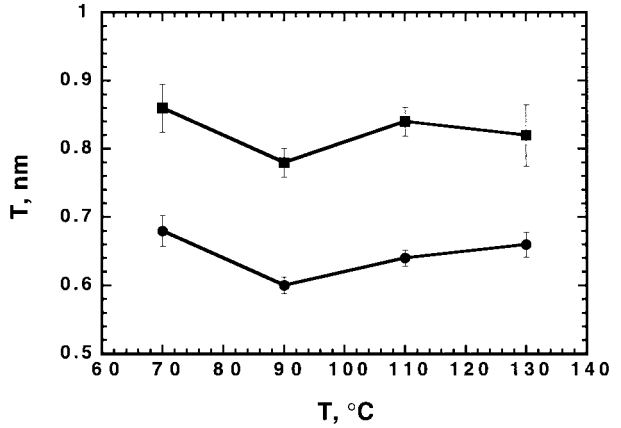

Figure 14. Plot of of species thickness, T, [^{l}T (■) and ^{c}T (●)] as a function of annealing temperature for all renatured samples 0P1 (error bars are standard errors).

^{l}T and ^{c}T for renatured sample 0P1 are shown in Figure 14. These thicknesses for the unsonicated sample are again independent of annealing temperature and indistinguishable from those of the several sonicated samples presented in Figure 13, this despite the significant difference in $^{l}T = T_n$ for the sonicated and unsonicated native material reported above.

Summary of NCAFM Observations. The observations reported above can be summarized as follows:

(1) The ratio N^{c}/N^{l} of cyclic to linear structures in the renatured samples is close to unity regardless of scleroglucan molecular weight in the range $4 \times 10^5 \leq M_w \leq 2.4 \times 10^6$. This ratio declines from about 2 to about 0.5 as the annealing temperature increases from 90 to 130 °C.

(2) Over this same temperature range, the mean contour lengths of the renatured structures, L_n, averaged over both linear and cyclic species, increase almost linearly with increasing annealing temperature for all the sonicated samples (1P2, 2P2, 3P3, 4P2); the temperature dependence of L_n is a little more complicated for the unsonicated sample (0P1), but the same increasing trend is observed.

(3) The mean contour lengths of the renatured cyclic species, ^{c}L, are consistently smaller than the mean contour lengths of the renatured linear species, ^{l}L, recovered from the same native precursor, provided the native material has been sonicated. Both ^{c}L and ^{l}L are effectively independent of temperature so that the increase in L_n with temperature reflects primarily a shift of the population from cyclic toward linear structures as annealing

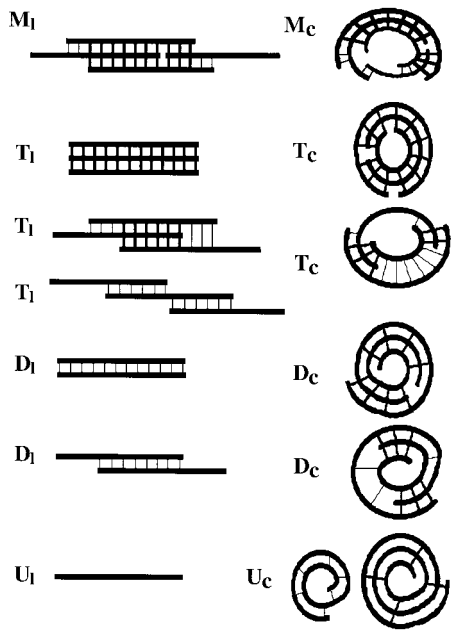

Figure 15. Schematic representations of the possible linear and cyclic clusters that can be formed from unimers of DP = 12.[54,61] Clusters are stabilized by helix stabilizing interactions conforming to the architecture of the scleroglucan triple helix described in Figure 2. Bold lines normal to chain axis correspond to triplex segments and thin lines correspond to duplex segments.

temperature increases. For unsonicated material, the mean contour length of the renatured cyclic species, ${}^{c}L$, exceeds the mean contour length of the renatured linear species, ${}^{l}L$, in the lower range of temperatures investigated.

(4) For the sonicated samples, the mean contour lengths of the renatured structures, L_n, averaged over linear and cyclic species, are smaller by about a factor of 2 than the mean contour lengths ${}^{l}L = L_n$ of their corresponding native precursors. For the unsonicated sample this factor is about 5.

(5) The sonicated native samples have mean thicknesses, ${}^{l}T = T_n$, that are only about 75% of the mean thickness, ${}^{l}T = T_n$, measured for the unsonicated precursor.

(6) The renatured linear structures have mean thicknesses, ${}^{l}T$, that are consistently 90−100% of the mean thicknesses of the corresponding native precursors, ${}^{l}T = T_n$.

(7) The mean thickness of the renatured cyclic structures, ${}^{c}T$, is consistently some 15−20% smaller than the mean thickness of the renatured linear structures, ${}^{l}T$. These thicknesses are sensibly independent of scleroglucan molecular weight and annealing temperature.

(8) Annealing of denatured samples for 4 h at temperatures ranging from 70 to 130 °C appears to be long enough for the NCAFM observable properties of this system to become stable. Only after considerably longer annealing times do irreversible changes in sample characteristics appear.

Interpretation and Conclusions

Cluster Diagrams. It is convenient to discuss the above observations with reference to the diagrams in Figure 15, where we depict the species that we imagine can be formed from fully or partially dissociated triple helices under renaturing conditions. The array of species includes linear and cyclic unimers (U_l and U_c), linear and cyclic dimers (D_l and D_c), linear and cyclic trimers (T_l and T_c), and various larger clusters that we designate generically as multimers (M_l and M_c). Each single chain depicted is taken to have 12 backbone glucose units each capable of forming a hydrogen bond at OH(2) with a backbone glucose unit in each of the other two chains in the scleroglucan triple helix (Figure 2). These hydrogen bonds, along with any other contributions to helix stability, are referred to here as "triplex-stabilizing interactions", or, more concisely, "interactions".

Any linear cluster containing two or more single chains must include duplex structure and may include triplex structure. Linear triplex (triple helical) structure is represented in Figure 15 by three parallel linear chains. Heavy lines drawn normal to the chain axes represent the triad of triplex-stabilizing interactions seen in Figure 2b at each level in the triple helix. Linear duplex (double helical) structure is formed by interaction of two parallel linear chains which lack a third parallel chain for completion of the triplex. Light lines normal to the chain axes in the duplex regions represent a single triplex-stabilizing interaction between the glucose units of two chains in triplex alignment. Duplex structure can be converted to triplex structure, with the formation of *two* additional interactions per segment of triplex, by addition of another chain to the cluster or by sliding (through a screw displacement) an existing chain of the cluster into juxtaposition with the duplex segment. Creation of two additional interactions upon formation of triplex from duplex structure introduces an important element of cooperativity into the cluster formation process that promotes triplex at the expense of duplex structure under renaturing conditions. Cyclic structures may also contain duplex and triplex segments. In this case, however, duplex and triplex structure can exist even in unimers, which contain just one polymer chain. Duplex and triplex regions of the cyclic clusters are depicted, as for the linear duplex and triplex regions, by light and heavy lines drawn normal to the local polymer chain axes.

The single chains depicited in Figure 15 are all imagined to be of the same DP; the polydispersity present in the experimental samples is not represented. Apparent differences in single strand length in Figure 15 are artifacts of the two-dimensional representation of three-dimensional objects. Specifically, all strands of the fully triplex linear trimer are equivalent because they are wrapped around a common helix axis; all strands of the fully triplex cyclic trimer are of the same length. Note that construction of cyclic unimers and dimers with large degrees of duplex and triplex structure necessarily involves some defects in the perfection of the ordered structure. Species depicted in Figure 15 do not include other possible structures that can be imagined, including those with parallel or otherwise overlapping strands but which lack triplex-stabilizing interactions between such strands.

It is clear from the diagrams that the contour lengths of linear and cyclic clusters are governed by the number of chains in the cluster and the degree to which the chains are involved in duplex and triplex structure. A fully triplex cyclic trimer has the same contour length as a fully triplex linear trimer, a fully duplex linear dimer, or a linear unimer. A cyclic dimer, when fully engaged in triplex structure has a contour length two-thirds that of a fully triplex linear or cyclic trimer, and only two-thirds as many stabilizing interactions can be formed. A completely triplex cyclic unimer has only one-third the contour length of the corresponding linear or cyclic trimer and has only one-third as many stabilizing interactions. The contour length of a cluster of given multiplicity increases as the extent of triplex and duplex structure is reduced. The mean thickness of a linear and cyclic cluster, averaged over the contour of the cluster, likewise depends on the number of chains in the cluster and the degree to which these chains participate in duplex and triplex structure.

Equilibrium States. It is interesting first to observe that the native scleroglucan is apparently not the thermodynamically stable form of the polymer, at least not at temperatures in the range 70 °C ≤ T ≤ 130 °C at which the denatured samples have been annealed. Denatured (unimeric or single strand random coil) scleroglucan, brought from high temperature denaturing conditions into the domain of Figure 3 where triple helix II is stable, spontaneously forms mixtures of linear and cyclic structures (and, at higher concentrations, more highly aggregated structures). Only linear structures are present in native material. This circumstance presumably accounts for the observed thermal irreversibility of the upper phase boundary in Figure 3.[26] Since the present samples are quenched quickly from the annealing temperature to room temperature for subsequent observation, we cannot be certain that, given time, the system would not equilibrate at room temperature to the fully linear, triple helical state; we can also not prove that the cyclic species are not just kinetic intermediates along the route to linear triple helical structure that have been trapped by the quenching process. The observed systematic increase of N^c/N^l with decreasing temperature suggests, however, that the system shifts in favor of the cyclic structures as the temperature declines (Figure 9). It is, thus, very tempting to speculate that the native scleroglucan isolated from its biological source is not in the thermodynamically most stable state. This is easily understood as a consequence of kinetic factors that favor formation of linear over cyclic forms under biosynthetic conditions (physiological temperature) where the process of triple helix formation is driven by a strong free energy gradient.

The very systematic changes in N^c/N^l and L_n with annealing temperature suggest rather strongly that quenching of annealed samples to room temperature arrests the kinetics of the association-dissociation process and reveals properties of the system that are close to the equilibrium state of the renatured system at the annealing temperature. As the annealing temperature increases toward the upper phase boundary in Figure 3, the equilibrium distribution of species can be expected to become more diverse and to contain less ordered (duplex and triplex) structure. As the temperature is raised, the free energy change driving formation of the (exothermic) triplex-stabilizing interactions is diminished, and both linear and cyclic renatured species can be expected to be less completely ordered or zipped up. The occurrence of significant stretches of uniplex and duplex structure increases the statistical likelihood that larger, and longer, clusters will form. It is easily shown that the concentration of multimeric clusters M_l and M_c is maximized at temperatures near the upper phase boundary.[61,66]

These arguments suggest that ${}^cL$ and ${}^lL$ might increase with annealing temperature. In fact, it appears for the sonicated samples to be only $L_n = N^{cc}L + N^{ll}L$ that increases with T for all sonicated samples investigated (Figure 10). This happens apparently because, even though ${}^cL$ and ${}^lL$ are approximately independent of temperature, ${}^lL > {}^cL$ and the ratio N^c/N^l decreases as temperature increases (Figures 8 and 9). Consistent with the temperature independence of ${}^cL$ and ${}^lL$, ${}^cT$ and ${}^lT$ also do not change with annealing temperature to within the precision of our measurements for any of the samples studied. This is perhaps also contrary to the expectation that the clusters should become less ordered with increasing T and therefore display decreasing ${}^cT$ and ${}^lT$ as annealing temperature is increased. An explanation for the constancy with annealing temperature of ${}^cL$ and ${}^lL$ and of ${}^cT$ and ${}^lT$ might be that the order−disorder transition is highly cooperative so that the transition approaches all-or-none behavior over a very narrow range of transition temperature.[67] The hypothesis of strong cooperativity is plausible for reasons already mentioned above, and some attempts at quantitative characterization of the cooperativity of the helix−coil transition in schizophyllan have been reported.[26]

Possible Polydispersity Effects. Remaining to be discussed are the reasons for the relatively strong decline of N^c/N^l with increasing annealing temperature. This might be a feature that arises from fractionation in the polydisperse system and that would not be apparent in a monodisperse sample. Figure 9 suggests, however, that both the sonicated and fractionated samples and the more polydisperse unsonicated sample display the same temperature dependence of N^c/N^l. It remains also to explain why, in contrast to the observations for the sonicated and fractionated samples, ${}^cL > {}^lL$ for the renatured unsonicated sample over most of the temperature range investigated (Figure 12). The unsonicated sample is more polydisperse than the sonicated, fractionated samples, and this might lead to a fractionation of the longer and more easily bent chains into cyclic structures.

This explanation implies that the unsonicated chains have contour lengths in a regime where longer chains have a greater propensity to cyclize than do the shorter ones. This is certainly true for chains of relatively short contour length for which cyclization encounters a strong energetic resistance to bending. The ring closure probability goes, however, as $\Lambda^{-3/2}$, where Λ is the contour length reduced by the Kuhn length,[68] for uniform single chains long enough to encounter little energetic resistance to cyclization. This result derives from the entropic barrier to ring closure first quantified by Jacobson and Stockmayer.[69] It does not incorporate the entropic advantage enjoyed by the cyclic structures that arises from the degeneracy of multiple-stranded cyclic forms.[14,28,29] In the case of triple helical scleroglucan, this advantage goes approximately as Λ^2. Thus, the overall ring closure probability increases approximately as $\Lambda^{1/2}$ in the limiting long chain length regime where flexional stress does not play an important role. For shorter chains, the ring closure probability increases even more rapidly with increasing Λ. Thus, on quite general grounds, we expect the ring closure probability to increase monotonically with Λ, and for polydisperse samples, it is reasonable to expect the longer chains to partition preferentially into the cyclic species.

The fact that ${}^cT < {}^lT$ consistently for all samples studied (Figures 13 and 14) may result from a deficit in ordered structure in the renatured cyclic species relative to the renatured linear species. Relatively less order in the cyclic species would be due to the free energy increment that arises from distortion of the idealized (linear) triplex structure on cyclization. This explanation implies that the mean contour lengths of the experimentally observed cycles fall in the regime of relatively small reduced contour length where energetic factors dominate the entropic factors in determining the ring closure probablility.[68] Under these conditions a cyclic cluster could reduce the flexional stress by being less ordered or zipped up than a linear counterpart. This would both increase the contour length and simultaneously reduce the effective persistence length (or chain stiffness) and thereby facilitate cycle formation. Measurements

(66) Washington, G. E. Ph.D. Dissertation Thesis, Univeristy of California, Irvine, 1987.

(67) Poland, D.; Scheraga, H. A. *Theory of Helix-Coil Transitions in Biopolymers*; Academic Press: New York, 1970.

(68) Shimada, J.; Yamakawa, H. *Macromolecules* **1984**, *17*, 689−698.

(69) Jacobson, H.; Stockmayer, W. H. *J. Chem. Phys.* **1950**, *18*, 1600−1606.

(70) Chuah, C. T.; Sarko, A.; Deslandes, Y.; Marchessault, R. H. *Macromolecules* **1983**, *16*, 1375−1382.

of mean chain thickness would then incorporate more domains along the contours of cyclic structures than of linear structures where the strandedness was less than 3. This would appear to account qualitatively for the observation that ${}^{c}T < {}^{l}T$.

If this reasoning is correct, then why is ${}^{c}L < {}^{l}L$ consistently for the sonicated and fractionated samples (Figure 11)? The above argument alone would suggest that ${}^{c}L > {}^{l}L$, because circles are less zipped up. The answer might be that the cyclic species are more likely to be dimers or unimers than are the linear species. To the extent that structures of the type U_c and D_c occur in the population of circles we expect ${}^{c}L < {}^{l}L$: Linear structures U_l, D_l, T_l and M_l can never have contour lengths less than that of U_l for monodisperse samples, if we make the approximation that a polymer repeating unit projects the same length on the chain contour in unimeric, dimeric, and trimeric segments. On the other hand it is entirely possible for the contour lengths of U_c and D_c to be less than that of U_l, as was noted above. One can wonder, however, if it is in fact possible for *monodisperse* samples to have simultaneously ${}^{c}T < {}^{l}T$ *and* ${}^{c}L < {}^{l}L$. Even if it is not, one must remember the role that polydispersity plays in the experimental system. The reason ${}^{c}L > {}^{l}L$ over most of the observed T range for the unsonicated, unfractionated sample 0P1 (Figure 12) might find its explanation in the higher mean chain length and greater polydispersity of this sample.

Possible Instrumental Artifacts. The origins of the observations that ${}^{c}L < {}^{l}L$ and ${}^{c}T < {}^{l}T$ for the sonicated and fractionated samples are perhaps more prosaic than the speculations just advanced. We have noted above that resolution in the NCAFM experiment in the *xy* plane parallel to the mica substrate is complicated by convolution of the sample thickness with the thickness of the probe tip. We see in Figure 4 (bottom), for example, that whereas the sample thickness measured in the *z* dimension is less than 1 nm, the apparent *xy* thickness (peak width at half-height) is of the order of 10 nm. This exaggeration will affect the *xy* dimensions of linear clusters measured longitudinally with respect to the cluster contour as well as those measured transversely as done in Figure 4. Hence, one should consider the measured values of ${}^{l}L$ to contain a systematic error of approximately +10 nm. Thus, for the smallest scleroglucan samples studied, 3P3 with ${}^{l}L \approx 125$ nm and ${}^{c}L \approx 95$ nm, the systematic error in ${}^{l}L$ is less than 10% and is sufficient to account for only a minor portion of the observation that ${}^{l}L > {}^{c}L$. This systematic error should be of relatively less importance for the larger scleroglucan samples.

Measurements of ${}^{c}L$, carried out as described above, are not subject to the same systematic error as measurements of ${}^{l}L$. It is possible, on the other hand, that the curvature of the cyclic samples displaces the high point in a topographic scan (e.g., Figure 4) across a cyclic structure toward the center of the cycle thus leading to a systematic error in ${}^{c}L$ of negative sign. We have no evidence for such an effect however, and the regular return of such scans to the baseline within the annuli of all but the smallest cycles (those with diameters of less that about 20 nm) suggests that we are able to measure accurately the high point on each limb of the cycles. An alternative explanation for why ${}^{c}T < {}^{l}T$ might reside in greater distortion, i.e., compression or compliance, of the cyclic structures by the attractive interactions with the mica substrate than would occur for the linear clusters, which presumably possess a higher degree of helical perfection than the cyclic clusters. This argument is perhaps not very different from the argument above that cyclic clusters are thinner because they tend to contain less duplex and triplex structure than their linear counterparts.

Several other observations are not subject to facile explanation within the present model. Why, for example, is native sonicated material measured to be only 75% as thick as native unsonicated material? Perhaps single strand nicks, which might be more common in the sonicated material due to free radical degradation, lead to greater chain compression from adhesive interactions with the substrate? Recall, however, the evidence from comparison of L_n before and after denaturation/renaturation that unsonicated native chains, which are thicker, have more nicks than sonicated native chains. Why also is the measured thickness of the unsonicated native material only about 67% that expected from the fiber diffraction model? Artifacts of measurement may be playing role here.

Acknowledgment. This work has been supported by NIH Research Grant GM 33062 to D.A.B., by NIH Traineeship Grant GM 07311-20 to TMM, and by ONR Research Grant 400X119YIP to Reginald M. Penner, whose generous advice and assistance with access to NCAFM instrumentation has made this work possible. We thank Hucheng Lee for performing light scattering measurements on scleroglucan fractions 0P1 and 4P2, Viscotek for light scattering experiments on 3P3, and Todd A. Talashek of NutraSweet/Kelco Co. for light scattering measurements on 3P3 and 0P1. We also acknowledge Michael D. Kirk of KAL-Tencor for valuable suggestions and Park Scientific Instruments for donation of some of the cantilevers used in this study. Finally, we thank B. T. Stokke and L. W. Gascoigne for offering valuable insights into the characteristics of this system.

JA981203E